XL CILAMCE
IBERO-LATIN AMERICAN CONGRESS ON COMPUTATIONAL METHODS IN ENGINEERING
NOVEMBER 11-14, 2019
Praiamar Natal Hotel & Convention
Natal, RN-BRAZIL

NUMERICAL STUDY OF AN ALUMINOTHERMIC REACTION BY A FOURTH-ORDER FINITE DIFFERENCE SCHEME WITH THE REACTION RATE MODELED AS CONSTANT AND BY THE N-ORDER METHOD

Kesiany Máxima de Souza
Marcelo José Santos de Lemos
kesianymaxima@gmail.com
delemos@ita.br
Instituto Tecnológico de Aeronáutica, Laboratório de Computação em Fenômenos de Transporte
São José dos Campos, Brasil

Abstract. Aluminothermic reactions have been widely applied in rail welding, pyrotechnics, and material synthesis, as they are highly exothermic. However, they are not easily modeled since they involve condensed phases, hardly result in gas products, and produce heterogeneous combustion waves where no thermodynamic equilibrium condition is attained. Moreover, the reaction rate of these reactions depends on particle sizes, oxidizer type, mixture ratios, and other physicochemical characteristics. So, major studies about aluminothermic reactions have been experimental, and just a few authors have tried to model the front propagation, shock generation and the kinetics of them. In this point of view, the present study aims to model the aluminothermic reaction between hematite and aluminum by solving the energy and mass conservation equations with a fourth-order finite difference scheme in space and first-order forward scheme in time. As there are not enough experimental studies about the activation energy and pre-exponential factor for this specific reaction, the reaction rate was modeled both as a constant and by the n-order method, which considers the dependence of reaction rate on temperature and species concentration and made it possible to observe the sensibility of these parameters. Moreover, the temperature dependence of density, specific heat capacity and thermal conductivity were considered in the model. The geometry and boundary conditions were based on experimental data from literature, which successfully enabled validation of the mean temperature and velocity propagation of the reaction.

Keywords: Thermite, Finite Difference Scheme, N-Order Method, Aluminothermic Reaction

1 Introduction

A thermite reaction, as shown in Eq. 1, refers to a class of reactions that involves a more active pure metal *M* reacting with a metal or non-metal oxide *AO*, resulting in a more stable oxide *MO*, a metal or non-metal *A*, and energy ΔH (Mei et al. [1]). It is a highly exothermic reduction-oxidation reaction with a production of great amounts of heat at high temperatures and a self-sustained behavior.

$$M + AO = MO + A + \Delta H \tag{1}$$

In order to understand the thermite's technological potential, we must start with its history. The discovery of the displacement of oxygen contained in metal oxides by aluminum is credited to Russian physicist Nikolay Beketov, who conducted experiments on aluminothermic reductions in 1865 at the University of Kharkov in Ukraine (Lunk [2]). Almost thirty years later, in 1893, the German Johannes Goldschmidt experimented with aluminothermic reactions to produce high purity chromium and manganese, which led him to patent the thermite process in 1895, and already in 1899 the thermite gained its first commercial application for rail welding in Essen, Germany, where the headquarters of the Goldschmidt Corporation was located. As a result, the advantages of thermite rail welding spread across Germany and around the world, leading to the inauguration of the Goldschmidt Thermit Company in New York in 1904 (Lonsdale [3]). In 1933, the first installation of open railroads was made using termite for welding on the Delaware and Hudson railroads in the United States (Archdeacon and Abbey [4]).

Note that in the first half of the twentieth century, the termite was mainly applied to rail welding. Already in the second half of the same century, it gained other applications that triggered various research. These include the invention of a power plant patented by Jhonson [5] where the driving fluid is heated by the termite reaction, the development of a high-regression-rate solid fuel composition by Allen [6], the development of methods for storing radioactive waste by Spector et al. [7], the aluminothermic production of metals and alloys (Belitskus [8]), the invention of a device that pierces metal targets patented by Marziano and Donnard [9], thermite use in the production of high pressure gases and velocities (Halcomb and Mohler [10]), thermite use in high temperature sintering and self-propagating (SHS) of ceramics and composite materials (Odawara [11]), the development of ignitors (Halcomb and Mohler [12]), and thermite application in the invention of a destructive device patented by Song [13].

Already in the 21st century, we have studies of new applications of thermite in challenging environments such as deep-water welding (Hagen [14]), and well sealing and abandonment (Skjold [15]), as well as the development of pyrotechnic compositions (Carter Jr and Carter [16]). With the development of nanotechnology, nanothermites have emerged which have been widely investigated for applications such as propulsive systems (Gangopadhyay et al. [17]), welding (Zanjani [18]), and well sealing (Hearn et al. [19]).

The physicochemical mechanisms that govern the thermite reaction are not completely understood. Although generally treated as a simple condensed-phase reaction, it is a highly complex process due to all the physical and chemical events involved such as phase changes, decompositions, surface tension, droplet collision, particle and heat transport (Weiser et al. [20]), among others, which make it difficult to model this type of reaction.

Therefore, we initially sought to simplify the reaction between hematite and aluminum presented in Eq. 2, which is one of the most common thermite reactions. Aluminum is the most widely used fuel in this type of reaction due to its high oxygen affinity, easy handling, high evaporation temperature, and abundance (Zanjani [18]).

$$Fe_2O_3 + 2Al \rightarrow 2Fe + Al_2O_3 \tag{2}$$

2 Governing Equations

To model the reaction propagation, temperature, and reagent consumption, the numerical model must solve the energy and mass conservation equations 3 and 5, respectively. Where ρ is the density, c_p is the specific thermal capacity at constant pressure, k is the thermal conductivity, S is the source term which accounts for the heat generated and thermal losses, W_A is the mass concentration of Fe_2O_3, α_A is the stoichiometric mass coefficient of Fe_2O_3, T is temperature, and r_r is the reaction rate.

$$\rho c_p \frac{\partial T}{\partial t} = \frac{1}{r}\frac{\partial}{\partial r}(r\frac{\partial T}{\partial r}) + S \tag{3}$$

$$\frac{dW_A}{dt} = \alpha_A r_{kr} \tag{4}$$

These governing equations were applied to the control volume experimentally analyzed by Duraes et al. [21] to validate numerical results. The reproduction of this control volume is shown in Fig. 1, where a thermite disc - hematite and aluminum -, 50 mm in diameter and approximately 1 mm thick, is comprised between a stainless steel plate and a PMMA cylinder with a hole in the center for ignition realization. Therefore, the numerical study performed is one-dimensional and considers the radial distribution of temperature and concentration of chemical species varying over time, for a thermite disc with a radius of 25mm.

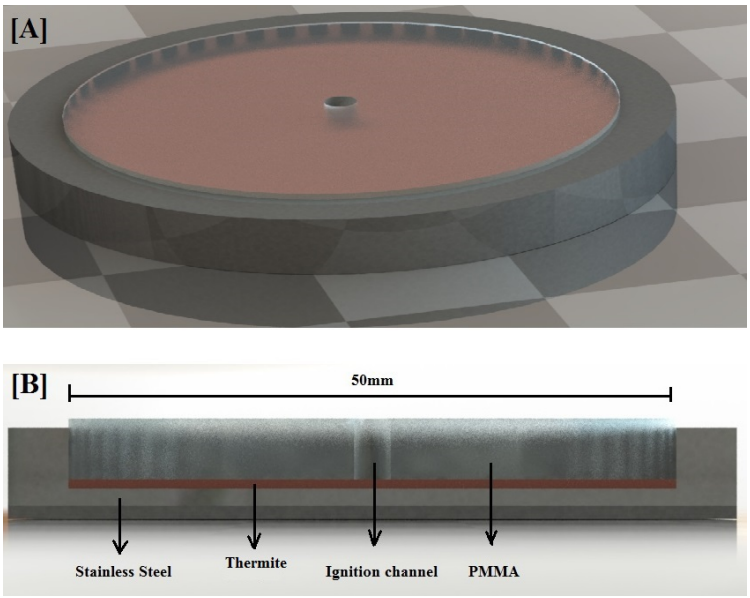

Figure 1. 3D reproduction of the experimental configuration of Duraes et al. [21] in trimetric perspective [A] and lateral view [B].

An overall temperature of 298 K was applied as the initial condition, together with reagent species concentrations at stoichiometric fractions, considering a medium porosity of 0.397 measured experimentally by Duraes et al. [21]. The boundary conditions account for an internal boundary (r = 0 mm) at symmetry condition, and an external boundary (r = 25 mm) with a given heat flux that accounts for convection, conduction, and radiation, as applied by Duraes et al. [22].

Overall, three cases were studied as shown in table 1. The first one considered a constant reaction rate equal to K, while the others considered the n-order kinetic model and the Arrhenius equation to determine the reaction rate. Notice that A is the pre-exponential factor, E_a is the activation energy, R is the ideal gas constant, T is temperature, W_{A0} is the initial mass concentration of Fe_2O_3, η_A is the reaction extension, and n is the kinetic order of the reaction. Therefore, case 1 does not consider the temperature and reaction extension effects in the reaction rate, while case 2 considers only the temperature effect, and case 3 considers both temperature and reaction extension.

Table 1. Methods applied to the reaction rate calculation.

case 1	$r_r = K$
case 2	$r_r = Ae^{-E_a/(RT)}W_{A0}(1-\eta_A)^n$, with n = 0
case 3	$r_r = Ae^{-E_a/(RT)}W_{A0}(1-\eta_A)^n$, with n = 1

3 Numerical Procedure

The domain was discretized in 201 nodes, with radial steps of $\Delta r = 0.125mm$. The numerical study is in the transient regime and, as so, the time steps are $\Delta t = 0.0001s$. The governing equations were then solved by a fourth-order finite difference scheme in space and first-order forward scheme in time. As so, they could be approximated by the algebraic Eq. (5) and (6), where i refers to the *ith* point in the domain, n to the *nth* time step, and A, B, C, D, and E are constants that depend on the time step Δt, radial step Δr, radius localization of the point r_i, and thermochemical properties of the mixture that were calculated as shown in Brito et al. [23].

$$A_i T_i^n = B_i T_{i+2}^n + C_i T_{i+1}^n + D_i T_{i-1}^n + E_i T_{i-2}^n + F_i \tag{5}$$

$$W_{A_i}^n = \alpha_A r_{kr} \Delta t + W_{A_i}^{n-1} \tag{6}$$

The thermite activation energy depends on several factors, such as reagent particle diameter, mixture compaction, and reagent ratio. Therefore, it is an experimentally measured value that varies according to its conditions. Fan et al. [24] reached 145 kJ / mol for the 8Al-3Fe2O3 reaction, and Rafiei et al. [25] reached the value of 82.3 kJ / mol for the reaction involving Al / Ti / Fe2O3, both using the method of Starink [26]. In the latter case, titanium may have influenced the decrease in activation energy. For the $2Al - Fe_2O_3$ reaction, no experiments were found in the literature that measured its activation energy. Therefore, iterative analysis of the activation energy was done and the highest value that allowed the self-propagation of the reaction was 60 kJ/mol. Then, with this activation energy, the pre-exponential factor for cases 2 and 3, and the constant kinetic rate for case 1, were varied in order to match the front propagation velocity of 26.9 mm/s measured by Duraes et al. [21]. Finally, the three cases modeled had the kinetic rate parameters set to the values shown in table 2.

Table 2. Parameters applied to the reaction rate calculation at each case.

case 1	$K = 49000\ kg/m^3 s$
case 2	$A = 2300\ s^{-1}$; $E = 60\ kJ/mol$
case 3	$A = 3700\ s^{-1}$; $E = 60\ kJ/mol$

4 Results

The front propagation of the reaction for all cases can be observed in Fig. 2, where the profiles of temperature and mass fraction of Fe_2O_3 are plotted at different times. The mean temperature reached after reaction is, approximately, 2300 K for all cases, which agrees with the temperature measured by Duraes et al. [21]. As so, the different models of the kinetic rate do not affect significantly the temperature reached. However, the initial propagation of the reaction front, from the inner boundary, is significantly slower in case 2, followed by case 3, when compared to case 1. This happens because, in case 1, the kinetic rate is constant since the ignition. In case 2, the kinetic rate does depend on the temperature and it takes some time to assume a pattern. The same happens to case 3, but it also has the influence of the extent of reaction, which results in a longer delay to the stabilization of the front propagation.

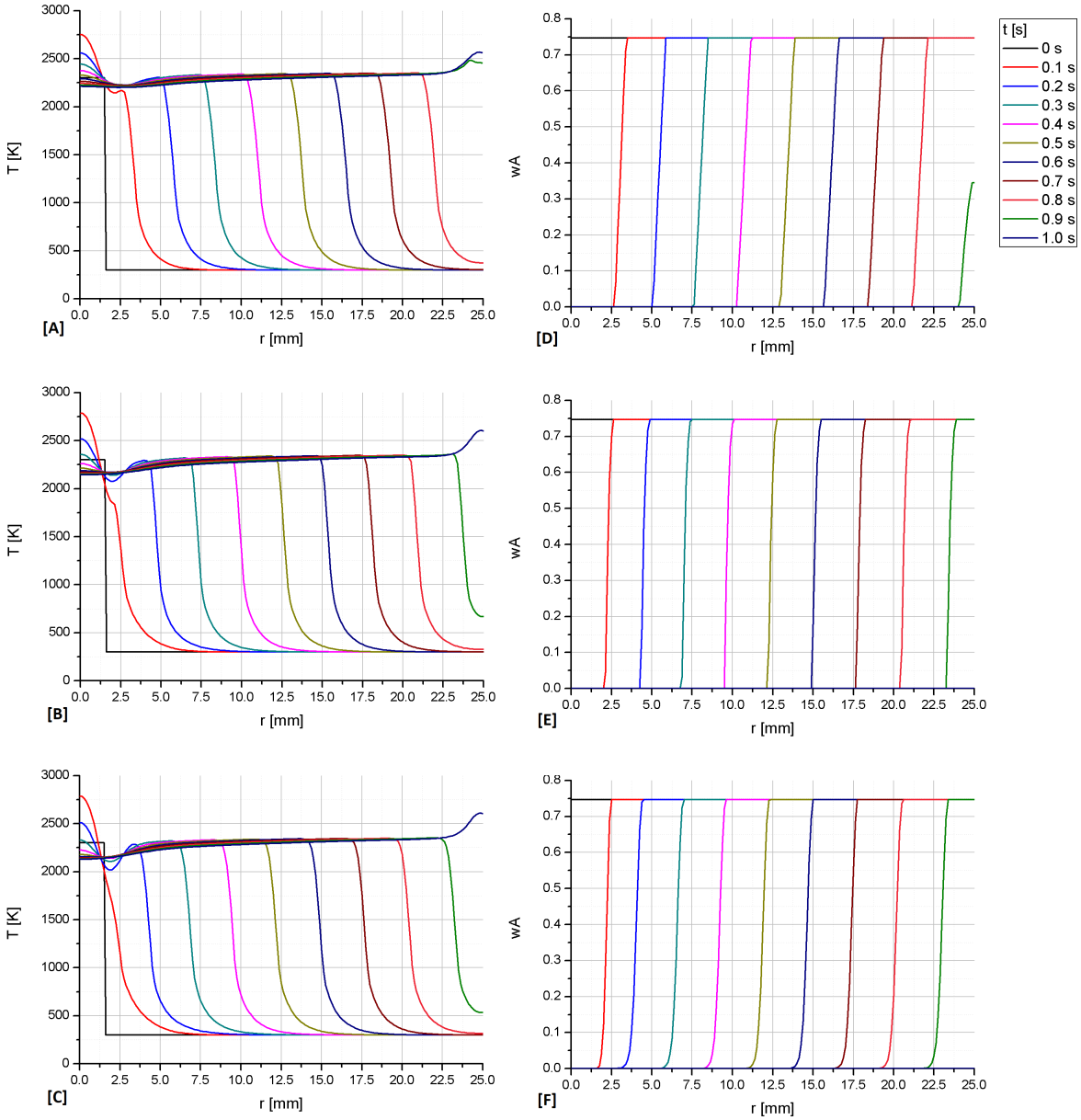

Figure 2. Temperature profiles of [A] case 1, [B] case 2, [C] case 3, and mass concentration of Fe_2O_3 profiles of [D] case 1, [E] case 2, and [F] case 3.

Fig. 3 shows the variation of propagation velocity through the domain for each formulation of the kinetic rate used. Speed was calculated according to the time it took for iron oxide concentration to fall by 50%. Note that all speeds reach an approximately constant value of 27 mm/s within the domain. The difference of the method used is significant only near the inner boundary of the domain, r = 0mm, where the results for case 1 shown a faster initial development of the front propagation than the other cases.

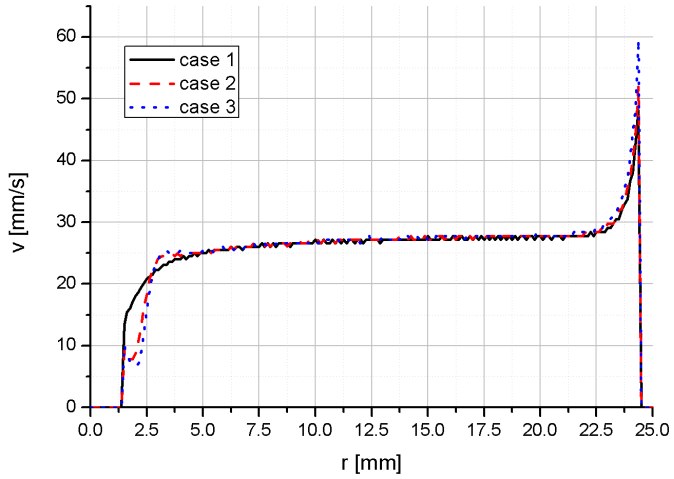

Figure 3. Velocity of the front propagation along the domain for all cases.

The effect of the different formulations of the kinetic rate is best observed in Figs. 4 and 5, which show the temporal variation of temperature and mass fraction of Fe_2O_3, evaluated at point r = 0.125 mm. Note in Fig. 4 that in case 3, the reaction-front takes a longer time to reach r = 12.5 mm, followed by case 2 and case 1, respectively. When the kinetic rate is considered constant, the reaction rate is the same from the ignition to complete reagent consumption. In the case of the first-order reaction that assumes a temperature dependence, the velocity is lower at the beginning of the reaction where temperatures are lower and increase exponentially with temperature. In the case where the reaction is of order 1, the reaction speed assumes a dependence not only on the temperature but also on the concentration of the reactants, which causes a reaction deceleration together with the decrease in the reactant concentration.

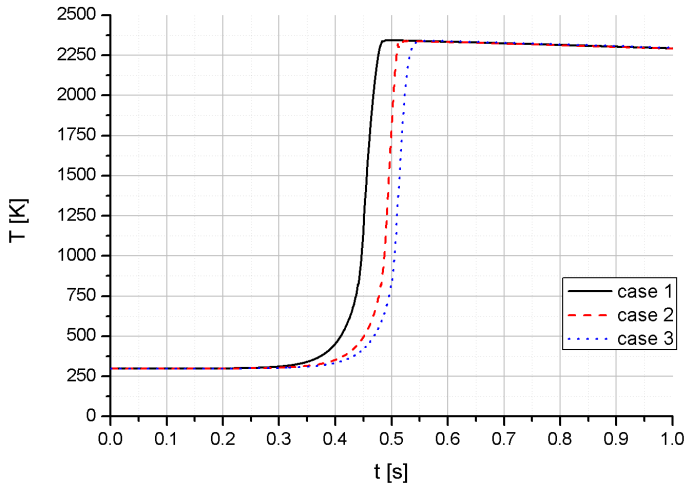

Figure 4. Temperature varying with time at $r = 12.5\ mm$ for all cases.

As seen in Fig. 5, with a constant kinetic rate, species consumption and production is linear. However, when using an exponential n-order formulation, the mass fraction variation profiles assume a non-linear behavior. The results for an order 0 kinetic rate only take into account the variation of the rate with the temperature, since the exponent of the species concentration is zero. The results for a 1st order kinetic rate assume a dependence not only on temperature but also on species concentration, the higher the concentration, the higher the rate, as explained before.

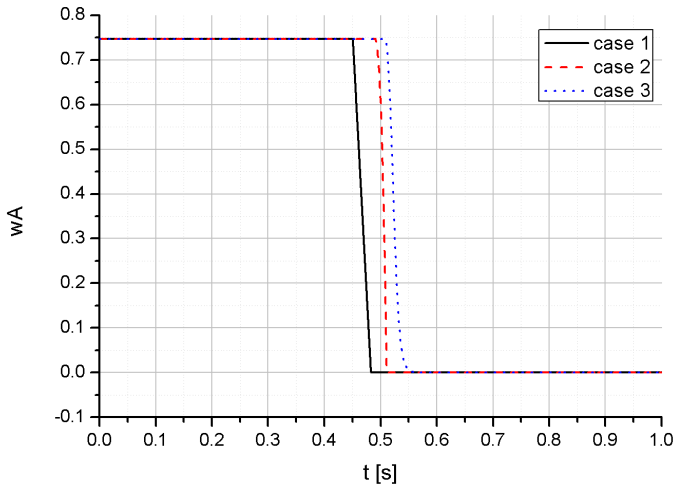

Figure 5. Mass concentration of Fe_2O_3 varying with time at $r = 12.5\ mm$ for all cases.

5 Conclusions

Despite many complex mechanisms involved in a thermite reaction, the present study could model a simplified hematite/aluminum reaction and solve the equations by applying a fourth-order finite difference scheme. The numerical results for temperature showed a good approach to the experimental results from Duraes et al. [21], with the front propagation velocity fitted to these experimental results. The reaction rate was modeled in three different ways, one considering a constant value, and others considering a dependence on temperature and reagent concentration. The results showed that as temperature and reagent concentration affects the reaction rate, the reaction-propagation takes longer to stabilize into a constant velocity. Moreover, the linear behavior in the consumption of reagent is lost when the kinetic rate is no longer constant.

Acknowledgements

The research was supported by the Coordination for the Improvement of Higher Education Personnel (CAPES), Brazil.

References

[1] Mei, J., Halldearn, R., & Xiao, P., 1999. Mechanisms of the aluminium-iron oxide thermite reaction. *Scripta Materialia*, vol. 41, n. 5, pp. 541–548.

[2] Lunk, H. J., 2015. Discovery, properties and applications of chromium and its compounds. *ChemTexts 1:6*.

[3] Lonsdale, C., 1999. Thermite rail welding: history, process developments, current practices and outlook for the 21st century. In *Proceedings of the AREMA 1999 Annual Conference*.

[4] Archdeacon, H. C. & Abbey, W. W., 1985. *The Track Cyclopedia*. Simmons-Boardman Books.

[5] Jhonson, D., 1970. Fuel unit for a gas turbine power plant. Patent US 3516880A.

[6] Allen, P. L., 1967. Thermite-resin binder solid fuel composition. Patent US 3309249A.

[7] Spector, M. L., Suriani, E., & Stukenbroeker, G. L., 1968. Thermite process for the fixation of high level radioactive wastes. *IEC Process Design and Development*, vol. 7, n. 1, pp. 117–122.

[8] Belitskus, D., 1972. Aluminothermic production of metals and alloys. *The Journal of The Minerals*, vol. 24, pp. 30–34.

[9] Marziano, S. J. & Donnard, R. E., 1980. Thermite penetrator device. Patent US 4216721A.

[10] Halcomb, D. L. & Mohler, J. H., 1990. High- and low-temperature-stable thermite composition for producing high-pressure, high-velocity gases. Patent US 4963203A.

[11] Odawara, O., 1990. Combustion and plasma synthesis of high temperature materials. Edited by Munir, Z. A., Holt, J. B. VCH, New York, pp. 179-185.

[12] Halcomb, D. L. & Mohler, J. H., 1991. Low profile thermite igniter. Patent US 4996922A.

[13] Song, E., 1997. Thermite destructive device. Patent US 5698813A.

[14] Hagen, N. C., 2000. Method and device for thermite welding at large water depths. Patent US 6131801A.

[15] Skjold, M., 2013. Method of well operation. Patent WO 2013/135583 A2.

[16] Carter Jr, G. & Carter, G., 2003. Pyrotechnic thermite composition. Patent WO 03/093402 A2.

[17] Gangopadhyay, S., Apperson, S., Gangopadhyay, K., Thiruvengadathan, R., & Bezmelnitsyn, A., 2011. Nanothermite thrusters with a nanothermite propellant. Patent US 2011/0167795 A1.

[18] Zanjani, G. B., 2013. Synthesis, characterization, and application of nanothermites for joining. Master's thesis, University of Waterloo, Waterloo, Ontario, Canada.

[19] Hearn, D. D., Hirschmann, C., & Shafer, R. S., 2018. Nano-thermite well plug. Patent US 2018/0094504 A1.

[20] Weiser, V., Roth, E., Raab, A., Juez-Lorenzo, M. M., Kelzenberg, S., & Eisenreich, N., 2010. Thermite type reactions of different metals with iron-oxide and the influence of pressure. *Propellants, Explosives, Pyrotechnics*, vol. 35, pp. 240–247.

[21] Duraes, L., Campos, J., & Portugal, A., 2006a. Radial combustion propagation in iron(iii) oxide/aluminum thermite mixtures. *Propellants, Explosives, Pyrotechnics*, vol. 31, n. 1, pp. 42–49.

[22] Duraes, L., Brito, P., Campos, J., & Portugal, A., 2006b. Modelling and simulation of fe2o3/aluminum thermite combustion: Experimental validation. In *16th European Symposium on Computer Aided Process Engineering and 9th International Symposium on Process Systems Engineering*.

[23] Brito, P., Duraes, L., Campos, J., & Portugal, A., 2005. Modelling and simulations of fe2o3/al thermite combustion. In *proceedings of CHEMPOR*, Coimbra.

[24] Fan, R. H., Lu, H. L., Sun, K. N., Wang, W. X., & Yi, X. B., 2005. Kinetics of thermite reaction in al-fe2o3 system. *Thermochimica Acta*, vol. 40, pp. 129–131.

[25] Rafiei, M., Enayati, M. H., & Farimzadeh, F., 2014. Kinetic analysis of thermite reaction in al-ti-fe2o3 system to produce (fe,ti)3al-al2o3 nanocomposite. *Powder Technology*, vol. 253, pp. 553–560.

[26] Starink, M. J., 1996. A new method for the derivation of activation energies from experiments performed at constant heating rate. *Thermochimica Acta*, vol. 288, pp. 97–104.